Journal of Materials Chemistry C

ROYAL SOCIETY OF CHEMISTRY

PAPER

View Article Online
View Journal

Cite this: DOI: 10.1039/d6tc00581k

Lasing from ordered colloidal micro-resonator arrays to random distributed systems

Konrad Cyprych, * Jastin Poplawski and Jaroslaw Mysliwiec

While colloidal microstructures are widely utilized to engineer ordered micro-resonator arrays with precise optical responses, intentionally harnessing their inherent structural randomness opens new ways for tailoring light–matter interactions. In this study, we investigate the profound impact of programmable structural disorder on the light-scattering and emission properties of colloidal micro-assemblies. Focusing on a dye-doped polymer system incorporating hollow silica microspheres, we demonstrate how controlled stochasticity alignment modulates the dominant optical feedback mechanisms. By manipulating surface tension-driven self-assembly, we observe a continuous morphological evolution from locally ordered, two-dimensional micro-gratings arrays to highly scattering macro-aggregates. Crucially, we show that increasing this structural disorder alters the light amplification pathway, transforming the optical emission sequentially, from distinct, localized resonant modes within well-defined cavities, through non-resonant amplified spontaneous emission (ASE), and ultimately culminating in robust random lasing (RL). Our findings underscore that integrating self-assembly principles with deterministically controlled randomness provides a powerful strategy to precisely engineer the emission regimes of photonic materials.

Received 24th February 2026,
Accepted 24th April 2026

DOI: 10.1039/d6tc00581k

rsc.li/materials-c

1. Introduction

The ability to precisely manipulate light–matter interactions at the micro- and nanoscale remains a central pillar of modern photonics, driving critical advancements in optical computing, telecommunications, and advanced sensing technologies.[1,2] Traditionally, this field has been heavily dominated by highly ordered architectures, such as photonic crystals and perfectly aligned micro-resonator arrays. These systems rely on strict spatial periodicity and structural perfection to confine and guide light *via* photonic bandgaps and high *Q*-factor resonators.[3,4] However, achieving and maintaining such flawless long-range order is often hindered by complex fabrication constraints and an inherent vulnerability to structural defects. Consequently, recent years have witnessed a profound paradigm shift toward disordered photonics, where inherent structural randomness is no longer viewed as an undesirable flaw, but rather harnessed as a powerful, functional resource for light manipulation.[5,6]

The widely studied manifestation of this concept is the random laser (RL).[7] Unlike conventional lasers, which require a highly precise optical cavity defined by macroscopic mirrors to trap light, RLs achieve coherent optical feedback through multiple scattering events within a disordered gain medium.[8,9] Since the foundational theoretical framework established by Letokhov and subsequent experimental validations, RLs have attracted immense scientific interest.[7,8,10] Their unique operating mechanism intrinsically produces emission with low spatial coherence, effectively eliminating undesirable laser speckle.[11,12] Among the diverse material platforms investigated for RL generation, colloidal micro-assemblies have emerged as highly versatile candidates. They offer a unique environment where the complex interplay between localized single-particle optical resonances and collective multiple scattering can be explored, setting the stage for advanced optical engineering.[13]

Despite the rapid maturation of both photonic crystal engineering and random laser physics, a fundamental challenge remains: achieving deterministic control over the intermediate states that bridge these two extreme optical regimes.[14] Historically, research paradigms have treated structural order and disorder as mutually exclusive properties. Consequently, optical systems are typically engineered to be either perfectly periodic to maximize bandgap effects or fully stochastic to optimize multiple scattering.[15,16] This binary classification leaves a critical gap in our understanding of correlated disorder and transitional morphologies, architectures that exhibit short-range order but long-range randomness.[17,18] While these intermediate states hold immense potential for tailoring light transport, they are frequently overlooked due to the difficulties in physically realizing and characterizing them in a controlled manner.

Soft Matter Optics Group, Wroclaw University of Science and Technology, Wyb. Wyspianskiego 27, 50-370 Wroclaw, Poland. E-mail: konrad.cyprych@pwr.edu.pl

A specific bottleneck in the current literature is the lack of a comprehensive framework linking the dynamic evolution of particle self-assembly to the resulting macroscopic optical feedback mechanisms. Most studies on random lasing rely on static, inherently disordered media, such as ground powders or fixed nanoparticle suspensions.[19] In such static systems, the transition from isolated, localized resonant modes to fully developed collective scattering is abrupt and difficult to engineer dynamically. Furthermore, the role of structural frustration, driven by factors such as particle polydispersity and solvent evaporation kinetics, as an active tool to control the transport mean free path of light remains largely unexplored.[20–23] Therefore, there is a pressing need for experimental and theoretical investigations that elucidate how controlled aggregation shifts the lasing paradigm, providing a much-needed bridge between micro-resonator physics and complex random media.

Recent advancements have increasingly highlighted the immense potential of exploiting engineered correlated disorder and dynamically tunable colloidal networks.[24] Contemporary studies demonstrate that actively managing spatial correlations within soft-matter assemblies yields highly tailorable light–matter interactions, successfully surpassing the fundamental limitations of static, macroscopic random media.[25] Furthermore, the latest breakthroughs in random laser engineering emphasize the critical role of transitional microstructures, where precise control over the localization transition and particle aggregation directly dictates the macroscopic optical feedback mechanism.[26–28] These recent paradigm shifts confirm that mastering the morphological evolution of complex scattering landscapes is essential for programming specific photonic emission profiles.

As a core element of can be listed colloidal nano- and microstructures, which in solution experience various interactions during fabrication, which depend on particle size, material composition, and the properties of the suspending liquid.[29,30] Self-assembly is driven by a complex interplay of forces, including surface tension,[31–33] van der Waals forces,[34,35] buoyancy, and electrostatic interactions.[36] The resulting spatial distribution of these particles minimizes the overall surface energy of the system.[37] Modelling this complex collective behaviour remains challenging, as it is akin to modelling the dynamics of magnetic microdisk systems.[38]

The resulting structures require robust characterization methods. Dominant approaches include diffraction techniques, such as laser diffraction,[39] and electron microscopy for direct visualization of the morphology. Mathematical descriptions, including the determination of structural parameters often derived from Delaunay triangulation or Voronoi diagrams, are essential for characterizing photonic crystals and predicting their optical properties.[40,41]

Hollow silica microspheres serve as an ideal functional building block for photonic integration. Their unique shell geometry and relatively low refractive index contrast with the surrounding polymer matrix allow them to function dualistically within the optical medium.[42] When isolated or loosely packed, the thin polymer layer coating the microspheres supports localized, high-quality whispering-gallery-mode (WGM)-like resonances.[43,44] However, as the particles aggregate, these microstructures transform into highly efficient stochastic scattering centers.[45] By systematically modulating the initial microsphere packing fraction, we demonstrate a deterministic and tunable transition from a regime dominated by isolated micro-resonator emission to one governed by macroscopic random lasing. This engineered structural frustration effectively transforms the active medium from a collection of uncoupled cavities into a complex, strongly coupled multimodal resonant network, providing a physical bridge between localized resonance and distributed optical feedback.[46]

In this work, utilizing hollow silica microspheres, we demonstrate how the disorder introduced to the colloidal micro-assemblies affects the structural morphology and the light amplification phenomenon. Furthermore, we show that it is possible to manipulate amplification conditions in a desirable manner. This provides clear insight into the transition from lasing in spatially ordered structures to the random lasing phenomenon, driven by modified light-scattering properties.

2. Materials and methods

Highly polydisperse hollow SiO_2 microspheres were utilized as the principal material to facilitate the manipulation of light scattering.[47] To construct the initial, ordered micro-resonator structures, these microspheres were subjected to size fractionation *via* multiple filtrations from an aqueous suspension. The resulting size-selected particles were employed to create planar, locally ordered micro-resonator arrays through self-assembly. Specifically, the fractionated spheres were dispersed in a 2% (w/w) solution of poly(methyl methacrylate) (PMMA, Merck) in chloroform, relative to the dry polymer mass. This suspension was then deposited onto a microscope slide and allowed to dry in air. The solvent evaporation drove the self-assembly process, forming a solid polymer matrix embedding the hollow silica microspheres. For light amplification and lasing experiments, active samples were prepared by incorporating 1% (w/w) Rhodamine 6G dye, relative to the dry polymer mass, into the matrix.

In contrast to the locally ordered arrays, heterogeneous samples were fabricated to intentionally introduce the structural disorder necessary for random lasing. These samples were created by mixing the raw, polydisperse hollow silica microspheres (MS) with PMMA and 1% (w/w) Rhodamine 6G dye in chloroform. By specifically omitting the size-fractionation step, the inherent broad size distribution of the microparticles (Fig. S1) frustrated ordered self-assembly.[20] Instead, this polydispersity promoted the formation of a randomly packed, highly scattering network. The weight ratio of microspheres to dry polymer mass was systematically varied from 0.25 : 1 to 1 : 1 (MS : PMMA), corresponding to a microsphere content of 20–50% (w/w). The mixture was spread onto a microscope slide and allowed to dry completely in air, ultimately resulting in a

solid polymer matrix containing dense, randomly distributed microsphere aggregates.

Basic characterization relied on optical techniques to assess the morphology and the degree of spatial alignment within the solidified polymer layers embedding the microspheres. Microscopic analysis in transmission mode, using 10× and 60× objectives, was employed to determine key morphological parameters and verify the structural arrangement. To quantify the macroscopic light scattering properties, coherent backscattering (CBS) measurements were performed using a HeNe laser (λ = 632 nm), a wavelength intentionally selected outside the absorption band of the Rhodamine 6G dye.[48] Analyzing the resulting backscattering cones enabled the extraction of the light transport mean free path (l_t), a critical parameter for evaluating the strength of multiple scattering and understanding the feedback mechanism in the highly disordered samples. Furthermore, to probe the spatial distribution and confirm the short-range periodicity of the locally ordered arrays, transmission diffraction patterns were acquired. For this purpose, the HeNe laser beam was loosely focused onto the samples, and the far-field diffraction patterns, indicative of the structures acting as 2D micro-gratings, were captured using a digital camera on a screen positioned 12 cm behind the sample.

Light amplification properties were investigated using a frequency-doubled Nd:YAG laser (Teem Photonics) emitting at 532 nm, delivering 600 ps pulses at a 100 kHz repetition rate. A frequency-tuned chopper, combined with a synchronized data acquisition system, was used to capture emission spectra averaged over every 10 pulses. To probe the emission from localized, locally ordered domains, a microscope (Nikon Ti2) equipped with a 10× objective was utilized for localized point excitation (Fig. 1(a)). Conversely, to investigate macroscopic random lasing driven by multiple scattering, the excitation beam was focused by a cylindrical lens into a 3.0 mm × 0.1 mm stripe (Fig. 1(b)), providing a sufficiently large gain volume. In both configurations, the excitation direction was strictly perpendicular to the incident light polarization. Emission spectra were recorded either with an Andor Shamrock SR163 spectrometer (equipped with an 1800 lines per mm grating) coupled to the microscope, or *via* an optical fiber during the stripe-like excitation experiments. The emission spectra were systematically analysed to determine the distribution of optical path lengths within the active medium. As described previously,[49,50] this was achieved *via* Fourier transform (FFT) analysis of the emission intensity mapped as a function of the wavevector. This mathematical approach enables the resolution of specific optical cavity lengths, allowing us to clearly distinguish between isolated local microresonators and the complex, strongly coupled scattering paths characteristic of random lasing.

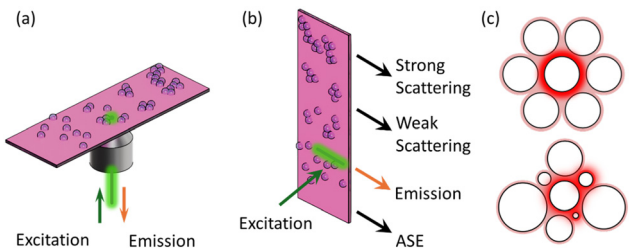

Fig. 1 (a) Point excitation setup for acquiring lasing from a precise location. (b) Excitation scheme utilizing a stripe-shaped beam, with distinct regions of strong and weak scattering, depending on the sphere density, and a scattering-free region exhibiting ASE. (c) Schematic of excitation from a localized hollow silica agglomerate with structured hexagonal alignment (upper panel) and spontaneously dispersed microspheres (lower panel), both embedded in a PMMA matrix containing Rh6G.

3. Results and discussion

Optical excitation of dye-doped polymeric layers is a well-established method for generating emission in random lasing systems. The combination of optical gain and structural inhomogeneities, such as aggregates, voids, or microparticles, provides the necessary scattering feedback to facilitate the random lasing phenomenon. In this study, we utilized hollow SiO_2 microspheres as these scattering centers, allowing us to dictate the lasing mechanism by controlling the spatial arrangement of the microparticles. By manipulating the collective morphology of these inclusions within the polymer matrix, it is possible to transition from structured, localized lasing originating from locally ordered micro-resonator arrays to macroscopic random lasing. The latter is driven by multiple light scattering governed by the structural heterogeneity of the highly disordered low-refractive-index centers, as conceptually depicted in Fig. 1(c).

The raw hollow silica microspheres used in this study exhibited a broad size distribution (Fig. S1) and were characterized with optical microscopy. The spheres displayed a well-defined spherical morphology, with their diameters following a broad distribution featuring two distinct maxima. The first maximum was centered around 13 μm and the second at approximately 50 μm, although sizes exceeding 150 μm were also occasionally observed. Such inherent polydispersity is highly advantageous, it not only actively frustrates long-range spatial ordering during self-assembly but also significantly enhances multiple light scattering within the Mie regime, both of which are crucial prerequisites for efficiently driving random lasing.[51]

To establish a baseline for the locally ordered microresonator arrays, a water-based microsphere suspension was allowed to sediment and was subsequently filtered repeatedly to size-fractionate the particles. This filtration process yielded a batch with a narrow size distribution, predominantly featuring diameters of approximately 6–8 μm (Fig. 2(a)). The resulting sediment was combined with a PMMA solution (with or without Rhodamine 6G dye) and cast into thin films. Driven by solvent evaporation, this approach yielded spontaneously organized two-dimensional patterns. While exhibiting localized order, these arrays also contained a degree of inherent randomness resulting from incomplete purification and the dynamic nature of the evaporation process (Fig. 2(b)). Consequently, these films displayed loose, short-range order with an average microsphere interparticle spacing of approximately 7.5 μm, effectively acting

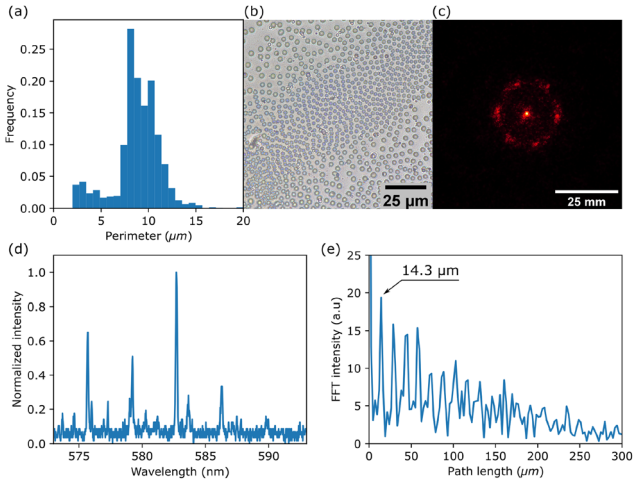

Fig. 2 (a) Perimeter histogram of the hollow silica microspheres embedded in the polymer layer. (b) Representative transmission optical micrograph of the locally ordered microsphere array within the PMMA matrix, and (c) the corresponding far-field diffraction pattern under loosely focused HeNe laser illumination, indicating short-range hexagonal alignment. (d) Emission spectrum demonstrating lasing action in a Rh6G-doped, locally ordered micro-resonator system, excited at 532 nm with a pulse energy of 1 μJ. (e) Optical path length calculated from the Fast Fourier Transform magnitude of the lasing spectrum, showing a fundamental harmonic at p = 14.3 μm, characteristic of the localized cavities.

as a 2D diffraction grating under HeNe laser illumination (Fig. 2(c)). The far-field diffraction patterns revealed a characteristic hexagonal alignment. Notably, in addition to the distinct diffraction spots corresponding to this hexagonal packing, a cubic orientation and a Debye ring was also clearly recognized (see Fig. S2). The emergence of the Debye ring is highly significant, as it indicates the formation of randomly oriented, locally ordered micro-domains that minimize the system's configurational energy,[39] thereby confirming the short-range, quasi-polycrystalline nature of the self-assembled grating rather than a globally perfect lattice.

Optical excitation of these locally ordered structures successfully produced lasing. Interestingly, even when employing a stripe-like excitation geometry to illuminate a larger area, the system yielded well-defined lasing originating purely from localized optical resonators (Fig. 2(d)), as evidenced by the narrow, well-separated emission peaks. The introduction of Rhodamine 6G dye into the PMMA matrix surrounding the microspheres effectively created an active medium populated by localized, low-refractive-index hollow inclusions. Consequently, light amplification was tightly confined to the high refractive index, dye-rich polymer regions distributed among the spheres (Fig. 1(c)). Analysis of the intermodal spacing with the FFT of the lasing spectrum revealed an optical path length of approximately 14.3 μm (Fig. 2(e)). Given that the average microsphere diameter is roughly 6 μm (corresponding to an equatorial circumference of ≈18.8 μm), this calculated path length explicitly confirms that the resonant feedback does not rely on standard Whispering Gallery Modes (WGMs) propagating around individual spheres. Instead, the lasing action is driven by coupled modes or complex localized paths strictly confined within the high refractive index polymer cavities bounded by the adjacent silica structures. The observed lasing remained spatially localized due to the short-range hexagonal alignment of these scattering centres. However, the overall emission intensity was notably lower than that observed from larger, highly disordered random lasing regimes. This limited signal strength is a direct consequence of the localized structural order, which supports efficient amplification only within isolated micro-domains. Simultaneously, this specific configuration severely inhibits efficient energy transfer and optical coupling between adjacent resonators across the macroscopic sample volume due to the lack of long-range periodicity. Perfectly periodic structures exhibit efficient phase-matched lasing across an entire sample,[52] whereas our locally ordered, weakly confined microstructures facilitate local amplification but inevitably lead to energy dissipation in the absence of global phase matching.[53]

Modifying the macroscopic scattering properties of the active layer is a well-established strategy for tuning random lasing (RL) emission characteristics.[54] In this work, we systematically enhanced multiple light scattering by deliberately incorporating unpurified, highly polydisperse hollow silica microstructures. The pronounced refractive index contrast served to strongly intensify the overall scattering strength within the active medium. Samples comprising a Rhodamine 6G dye-doped PMMA matrix were prepared with varying microsphere weight fractions ranging from 20% to 50%. During solvent evaporation, capillary forces and surface tension typically drive colloidal self-assembly, however, the inherent broad size distribution of our microparticles actively frustrated the formation of long-range ordered lattices. Instead, this frustrated self-assembly induced the formation of dense, spatially irregular aggregates. Consequently, the layer exhibited a complex, heterogeneous morphology: macroscopic domains of highly scattering, densely packed microsphere clusters were distinctively interspersed among contiguous regions of gain-rich, dye-doped polymer. The polydisperse nature of the microspheres ensured that smaller particles effectively filled the interstitial voids between larger ones, optimizing the random packing density to minimize the overall surface energy of the system. This dense, stochastically packed architecture is critical, as it maximizes the scattering cross-section and facilitates the intricate optical feedback network fundamentally required for efficient random lasing.

Microscopic imaging reveals that in regions of lower scatterer density, thin polymer layers bind individual microspheres while maintaining distinct inter-particle spacing (Fig. 3(a)). These interstitial voids are primarily occupied by the dye-doped PMMA, providing the highly localized active volumes necessary for light amplification within isolated micro-cavities. Furthermore, capillary bridges, indicative of polymer accumulating between adjacent spheres during the final stages of solvent evaporation, were observed, consistent with previous reports.[55] As the microsphere density increases, the morphological dynamics shift significantly. The dye-containing polymer

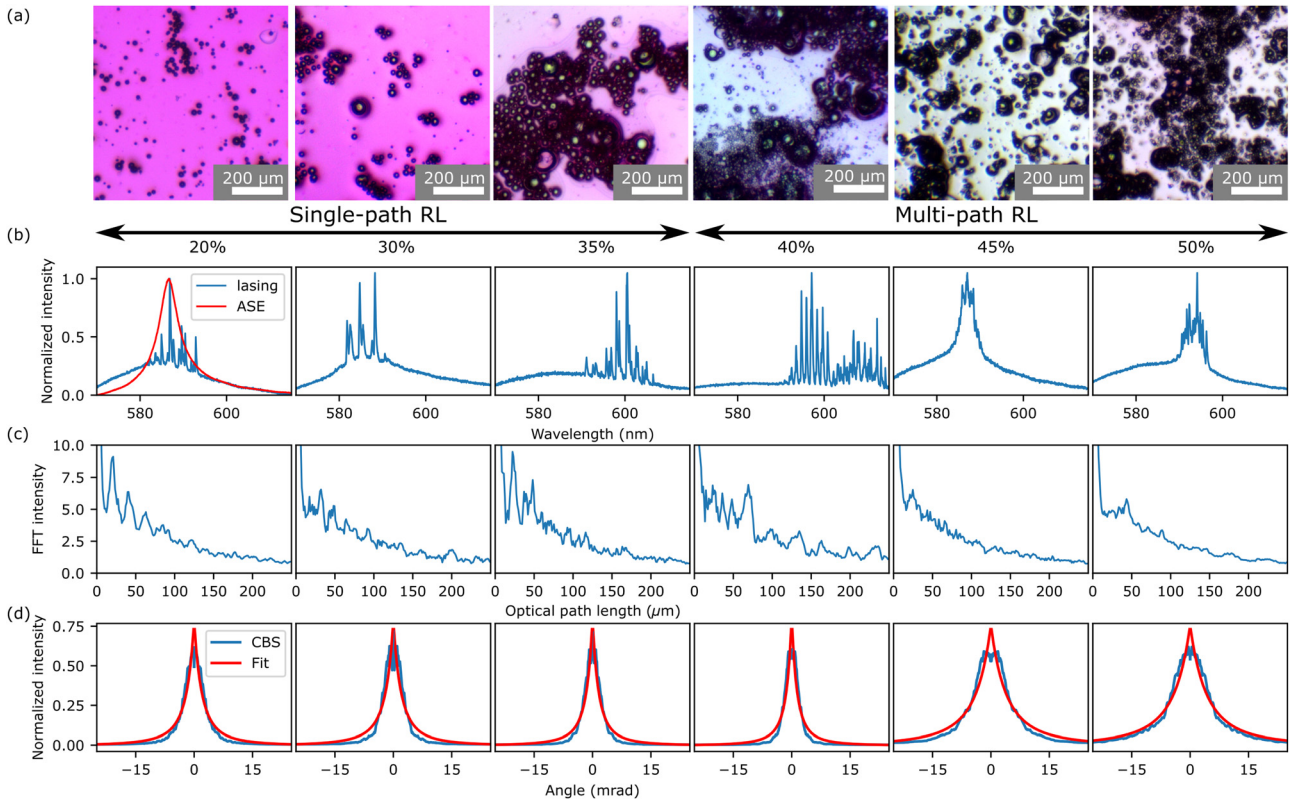

Fig. 3 Evolution of structural and optical properties driven by increasing structural disorder. (a) Transmission optical micrographs illustrating the morphological transition from loosely packed microspheres to dense, randomly distributed aggregates as the scatterer concentration increases. (b) Representative emission spectra acquired under localized excitation for samples with 20–50% (w/w) microsphere content. In regions with lower scatterer density, the lack of sufficient optical feedback predominantly results in broad ASE. (c) Averaged Fast Fourier Transform amplitude spectra of the emission, revealing the transition from distinct, localized micro-resonator modes to a complex strongly coupled scattering paths characteristic of random lasing. (d) Coherent backscattering cones and corresponding fits, reflecting the change in the scattering regime associated with enhanced multiple scattering.

matrix increasingly infiltrates and surrounds the densely packed clusters. Because the internal surface area of these three-dimensional microsphere aggregates vastly exceeds that of the flat underlying substrate, capillary forces effectively draw the polymer upwards into the complex spatial network of the clusters. Consequently, the continuous polymer film on the underlying substrate is severely depleted, and the available optical gain volume becomes almost exclusively confined within the aggregates themselves. Rather than being a limitation, this process is highly advantageous, it ensures an intimate spatial overlap between the active gain regions and the strong Mie scattering centers. This morphological arrangement creates the ideal physical environment to support efficient multiple scattering feedback, ultimately driving the transition to macroscopic random lasing.

The transmission micrographs in Fig. 3(a) clearly illustrate this morphological transition, highlighting the profound changes in both the aggregate architecture and the spatial distribution of the active surrounding medium. The progressive formation of these randomly distributed, dense microsphere clusters drastically alters the macroscopic light-scattering conditions, which consequently governs the observed laser emission behaviour (Fig. 3(b)). At a relatively low microsphere content (20%), lasing primarily originates from isolated, well-defined optical micro-resonators formed within locally ordered domains. This localized feedback is distinctly evidenced by the highly structured lasing spectra and the corresponding FFT magnitude, which presents sharp, well-defined fundamental harmonics (Fig. 3(c)). Conversely, in highly diluted regions with very few scatterers, broad amplified spontaneous emission (ASE) was observed without the buildup of discrete optical resonances. Under these sparse conditions, even macroscopic stripe excitation merely enhanced the spontaneous emission rather than triggering random lasing. This indicates critically insufficient optical feedback, a characteristic limitation of isolated or weakly coupled scatterers. In such regions, optical amplification occurs strictly within the bulk polymer layer as light travels through it, but it inevitably escapes the medium before forming the closed multiple-scattering loops necessary to sustain lasing action.

Increasing the microsphere content into the intermediate regime of 30–40% facilitates the onset of robust random lasing under both macroscopic stripe-beam and localized microscopic excitation. This emission arises from the simultaneous activation and optical coupling of multiple adjacent micro-resonators within the growing aggregates. This multi-cavity coupling is

explicitly demonstrated at the 40% concentration, where the emission originating from two spatially distinct optical resonators, represented by gain profiles separated by approximately >15 nm, simultaneously exhibits entirely distinct free spectral ranges and overlapping gain profiles (Fig. 3(b)). As the microsphere concentration is further increased towards 50%, strong multiple light scattering completely dominates the optical feedback mechanism. This highly disordered regime supports an immense number of spatially overlapping, stochastic lasing modes. Consequently, the sheer spectral superposition of unresolved emission peaks covers the individual sharp resonances, yielding a broad, continuous emission profile that closely mimics an ASE-like spectrum. Under these intense multiple-scattering conditions, the averaged FFT amplitude loses its discrete, well-defined harmonics and transitions into a broad, continuously fluctuating response. This mathematical signature definitively confirms that the emission is no longer sustained by isolated optical cavities.

Correlating the microscopic imaging, lasing emission characteristics, and coherent backscattering (CBS) data (Fig. 3(d), Fig. 4(a)) reveals a profound structural and optical transition driven by the microsphere concentration. In the lower concentration regime (<35%), the transport mean free path (l_t) remains relatively constant at approximately 20 μm, reflecting scattering events dominated by isolated, locally ordered micro-domains and individual scatterers. Interestingly, as the concentration exceeds 35%, l_t exhibits a transient increase. This behavior suggests the initial formation of distinct, denser aggregates separated by broader, scatterer-free polymer regions, which temporarily extends the average distance photons travel between bulk scattering events. However, a further increase in scatterer content (>45%) leads to a sharp, subsequent decrease in l_t. This critical drop implies a morphological shift into a densely packed, highly disordered macroscopic regime, explicitly corroborated by the microscopic imaging (Fig. 3(a)). Ultimately, this non-monotonic evolution of l_t perfectly captures the system's morphological transition, starting from loosely distributed localized domains, transitioning through a phase of isolated macro-cluster formation, and finally saturating as a strongly scattering, interconnected stochastic medium perfectly tailored to support robust random lasing.

During the initial stages of film formation, the dispersed microspheres undergo continuous Brownian motion within the polymer matrix. As the solvent progressively evaporates, capillary forces and surface tension strongly drive the aggregation of the free microparticles. However, driven by the inherent polydispersity of the spheres, perfect long-range crystallization is frustrated; instead, this process yields massive, spatially distinct clusters characterized by a densely packed, stochastic internal architecture. This pronounced aggregation drastically reduces l_t, as the overall optical transport becomes heavily dominated by strong multiple scattering events confined within these macroscopic aggregates, which inherently possess very short intra-aggregate scattering path lengths. Continually increasing the microsphere concentration does not fundamentally alter this internal stochastic packing morphology, rather, it significantly expands the overall volume and interconnected of the individual clusters. Ultimately, this structural evolution drives l_t down to a minimum of approximately 10 μm while simultaneously maximizing the macroscopic heterogeneity of the system (Fig. 4(a)). It is precisely this structurally induced randomness that governs the observed transition to macroscopic random lasing. At the highest evaluated microsphere concentration (50%), l_t reaches its minimum, fundamentally altering the emission characteristics. The overall emission intensity increases significantly (Fig. 3(b)), driven by a highly complex optical feedback network.

A fundamental evaluation of the lasing threshold was performed to quantify the influence of structural composition on the system's emission characteristics. We observed a systematic evolution in the lasing performance as a function of hollow scatterer density within the polymer matrix. As depicted in Fig. S4, and collectively summarized in Fig. 4(c), the energy threshold required to initiate laser action exhibits a clear inverse correlation with the scatterer concentration. Specifically, the threshold markedly decreases from an initial 285 μJ cm^{-2} to below 200 μJ cm^{-2} at higher packing fractions.

This progressive threshold reduction is primarily driven by the intensification of multiple scattering events, which facilitates the spatial coupling and coherent accumulation of emission signals from an expansive network of stochastic resonators. In contrast, the filtered samples demonstrate a significantly lower

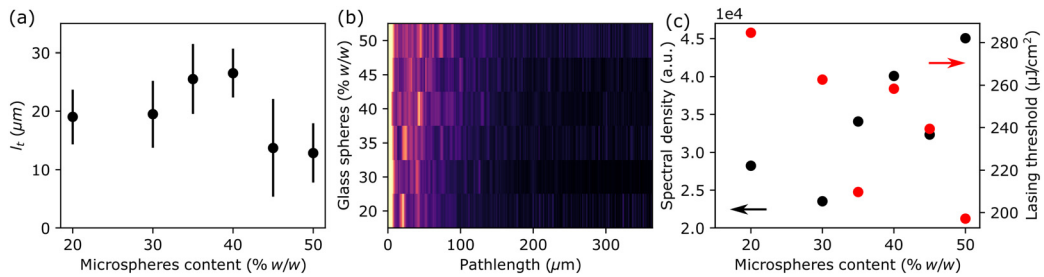

Fig. 4 Correlation between macroscopic scattering strength and the transition in emission characteristics. (a) Mean transport path length (l_t) as a function of microsphere content, obtained from coherent backscattering measurements, illustrating the onset of strong multiple scattering at higher particle concentrations. (b) Impact of increasing microsphere content on the FFT magnitude, highlighting the shift from a few dominant, localized micro-resonator modes to a broad, continuous distribution of coupled optical paths. (c) Spectral density parameter, derived from the FFT analysis of the normalized emission spectra, combined with lasing threshold.

lasing threshold of approximately 125 μJ cm^{-2}. This behavior confirms that long-range structural order promotes the formation of discrete, high-Q micro-cavities, which sustain more efficient optical feedback compared to the collective scattering mechanisms dominant in the disordered phase.

Distinguishing between isolated, single-loop resonances and complex, multi-path random lasing is crucial for understanding the observed spectral evolution. This fundamental transition can be effectively visualized by analyzing the distribution of optical path lengths contributing to the emission, as derived from the Fast Fourier Transform (FFT) analysis presented in Fig. 3(c) and 4(b). The enhanced multiple scattering inherently supports emission from significantly longer, more intricate optical pathways. Consequently, the overall FFT amplitude broadens and increases, reflecting a dramatically higher spectral density within the random lasing emission.[13,56] This physical relationship can be mathematically defined as:

$$S = \frac{\int |\mathscr{F}\{I(\lambda)\}| \mathrm{d}p}{\int I(\lambda) \mathrm{d}\lambda} \quad (1)$$

where S defines the spectral density parameter, $I(\lambda)$ represents the lasing emission intensity, and $|\mathscr{F}\{I(\lambda)\}|$ denotes the absolute magnitude of the Fourier transform of the emission spectrum. The numerator integrates the FFT magnitude over the optical path length, p, capturing the total contribution of all active resonant cavities. The denominator integrates the raw emission spectrum over the wavelength, λ, effectively normalizing the spectral density against the total emitted energy to ensure robust comparability across varying scattering concentrations.

The calculated increase in the spectral density parameter, S (Fig. 4(c)), provides robust quantitative support for the profound transition from localized, well-defined micro-resonators to a fully developed random lasing regime as the microsphere content increases. This trend demonstrates the broad tunability of the emission characteristics achievable strictly through the deliberate control of the scatterer density and resulting morphology. To definitively validate this scattering-driven mechanism, a reference sample consisting of a smooth, neat PMMA layer doped solely with Rhodamine 6G dye was evaluated. As expected, lacking any internal scattering centers, this control film exhibited purely spontaneous fluorescence under focused microscopic point excitation, and merely transitioned into amplified spontaneous emission (ASE) when subjected to macroscopic stripe-like beam excitation. Sustained lasing action fundamentally requires robust optical feedback, typically provided either by external cavity mirrors or, in the case of random lasing, by a sufficiently complex scattering medium to facilitate multi-path light recirculation. In the presented system, the introduced microspheres provide the exact localized structural inhomogeneities required to overcome the simple ASE threshold and successfully drive the transition into a highly efficient, multiple-scattering lasing regime.

The intricate interstitial voids strictly bound by the adjacent microspheres, which are continuously occupied by the thin active layer of dye-doped polymer, serve as the primary regions for light amplification. Rather than forming simple one-dimensional standing waves, highly complex, localized optical resonant modes manifest within these strongly confined, high refractive index micro-cavities. These localized modes effectively drive the lasing action in direct synergy with the intense optical gain provided by the concentrated dye. The ultimate stochastic morphology of these aggregates is governed by a delicate interplay of several concurrent kinetic and thermodynamic processes. Initially, the continuous Brownian motion of the suspended microspheres dictates their highly stochastic spatial distribution. Subsequently, as the solvent undergoes complete evaporation, dynamically evolving capillary forces and surface tension at the polymer–air interface aggressively drive the microparticles to cluster together. Ultimately, the definitive architecture of these densely packed structures is dictated by a complex, final equilibrium balancing these interfacial phenomena with competing electrostatic, buoyant, and van der Waals forces. It is precisely this intricate contest of forces, combined with the inherent polydispersity of the scatterers, that successfully frustrates perfect long-range order and yields the robust random scattering medium.

From the fundamental perspective of light amplification, a profound dichotomy exists between the emission profiles generated by locally ordered architectures and those characteristic of fully developed random lasing. As previously established, a hexagonal arrangement of inclusions inherently promotes the confinement of light into sharp, discrete, and isolated resonant modes. Conversely, systematically increasing the scatterer concentration deliberately disrupts this local order. This drives a macroscopic morphological transition that fundamentally alters the optical feedback mechanisms, ultimately yielding a broad, stochastic random lasing profile. To theoretically validate this concentration-driven morphological evolution and to accurately model the complex kinetics underlying this frustrated self-assembly and aggregate formation, we employed comprehensive rigid-body simulations.

The rigid-body simulations were initialized by assigning a random initial velocity vector to each particle to emulate thermally driven Brownian motion. To model the progressive cohesion of the microparticles, we introduced an effective damping mechanism that explicitly dictates the loss of kinetic energy during inelastic collisions. This phenomenological approach utilizes an attenuation parameter, σ, to simulate the complex dissipative interactions governing the macroscopic aggregation process. Based on the conservation of linear momentum for equal-mass objects, the post-collision velocity vector of the i-th body, $\vec{u}_i$, upon contact with the j-th body is defined as:

$$\vec{u}_i = \vec{v}_i - \sigma \frac{(\vec{v}_j - \vec{v}_i) \cdot (\vec{r}_j - \vec{r}_i)}{|\vec{r}_j - \vec{r}_i|^2} (\vec{r}_j - \vec{r})_i \quad (2)$$

where σ represents the dimensionless attenuation parameter, $\vec{v}$ denotes the pre-collision velocity vector, and $\vec{r}$ indicates the spatial position vector. For fundamental simplicity, a uniform constant mass was assumed for all simulated objects. The parameter σ essentially serves as a macroscopic numerical

proxy for the microscopic energy dissipation driven by cohesive capillary and van der Waals forces during real particle collisions. Because the dynamic evolution of surface tension during actual solvent evaporation is profoundly complex, explicitly modeling these transient fluid dynamics would be computationally prohibitive and phenomenologically unnecessary for capturing the final structural states. Therefore, we strategically constrained our investigation to a parametric sweep of σ. The simulation environment was initialized with non-overlapping circular bodies occupying an initial packing fraction of 5% of the total simulated 2D domain.

Throughout the simulation, the structural evolution was quantitatively monitored using the aggregation parameter, A, defined as: $A = N_A/N$ where N represents the total number of particles in the system and N_A denotes the number of particles identified as aggregated (defined by a spatial proximity criterion representing physical contact). Systematically altering the attenuation parameter, σ, was found to exert a profound influence on both the equilibration kinetics, specifically the time constant required to reach a stable morphology (Fig. 5(a)), and the maximum steady-state aggregation degree achieved by the system (Fig. 5(b)).

The rigid-body simulations successfully replicate the transition toward macroscopic aggregation. For the boundary case of $\sigma = 1$, representing perfectly elastic collisions with no energy dissipation, Fig. 5(a) exhibits only minimal, transient clustering. This marginal aggregation value arises solely from the stochastic, short-lived proximity of particles during elastic interactions rather than stable bond formation. However, as the attenuation parameter σ decreases (reflecting increased energy dissipation), the system reaches a stable, elevated aggregation equilibrium more rapidly, as evidenced in Fig. 5(b). Consequently, the characteristic size and density of the resulting aggregates are intrinsically governed by the dissipative forces acting during the assembly process. These numerical findings strongly correlate with the experimentally observed

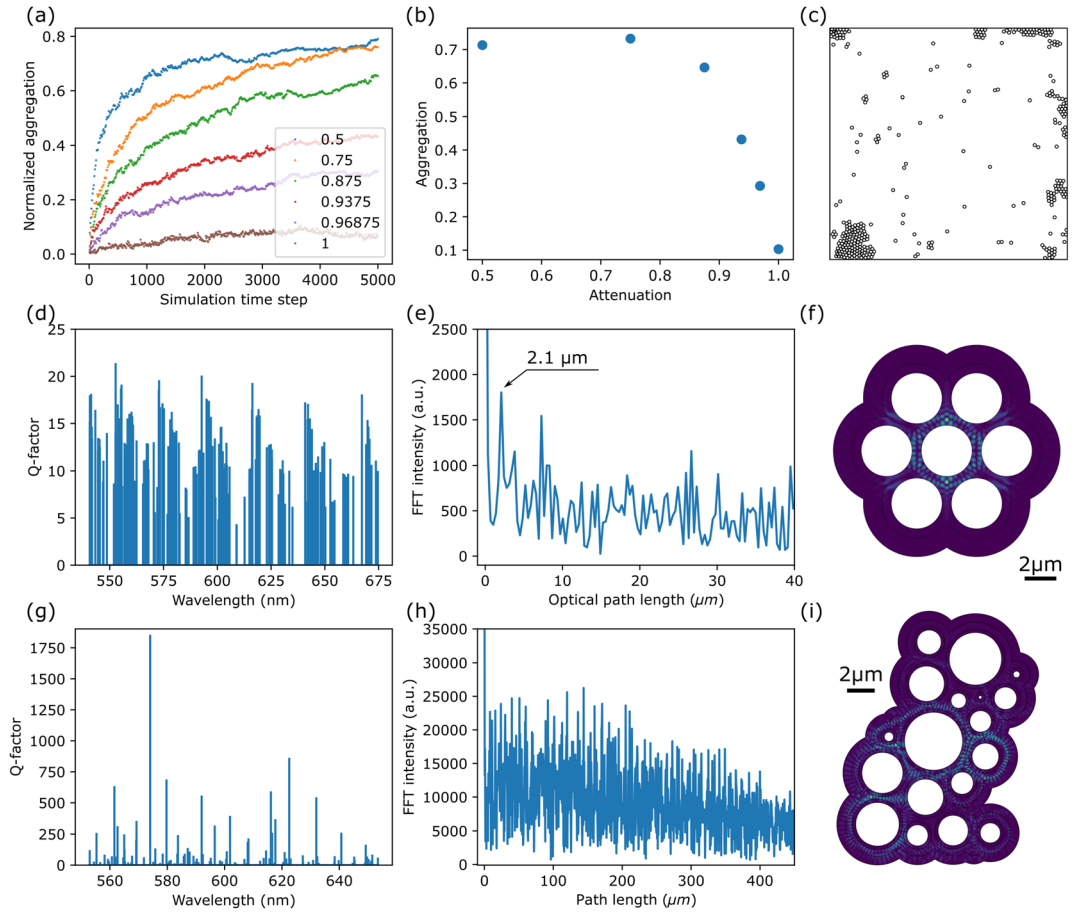

Fig. 5 Theoretical modeling of structurally driven aggregation and the corresponding transition in optical feedback mechanisms. (a) Temporal evolution of the normalized aggregation parameter (A) calculated for varying interaction attenuation parameters (σ). (b) Steady-state amplitude of the aggregation parameter as a function of σ, illustrating the critical threshold for the formation of dense clusters. (c) Representative 3D morphology generated *via* rigid-body simulations (σ = 0.5), successfully mimicking the experimentally observed stochastic aggregates induced by frustrated self-assembly. FDTD simulations for (d–f) a locally ordered hexagonal array and (g–i) a highly disordered, random arrangement of microspheres. (d and g) Simulated cavity Q-factor spectra for both structural regimes. (e and h) FFT derived from the respective Q-factor datasets, confirming the shift from discrete, isolated resonances in the ordered array to a broad continuum of coupled modes in the disordered aggregate. (f and i) Calculated spatial light intensity distributions. Panel (f) demonstrates spatial confinement of optical modes, whereas panel (i) reveals the extended, complex multiple-scattering networks.

effects of the solvent evaporation rate in polymer-microsphere composites. Even under the simplifying assumption of uniform particle size, the simulation suggests that the rate of solvent removal, which physically dictates the damping of particle motion *via* evolving viscosity and interfacial tension, is the primary kinetic driver determining the final stochastic morphology of the random scattering medium.

Once stabilized within the dye-doped polymer matrix, the hollow silica microsphere aggregates function as sophisticated optical resonators, where the surrounding polymer serves as the active gain medium. These dispersed glass microstructures play a dual role, acting simultaneously as discrete resonators and stochastic scattering centers. This configuration facilitates two distinct, concurrent feedback mechanisms: localized, WGM-like resonance within the thin polymer layer coating the microspheres, and distributed feedback arising from multiple light scattering off individual particles and their larger clusters. In particular, the extensive aggregates support highly intricate electromagnetic field distributions. This multi-scale architecture effectively bridges the gap between individual resonant modes and collective scattering phenomena, thereby giving rise to the robust random lasing behavior observed in the system.

To quantitatively model these phenomena, rigid-body simulations employing a realistic normal particle size distribution were utilized to generate representative stochastic aggregates depicted in Fig. S3. Subsequent finite-difference frequency-domain (FDFD) analysis of these simulated structures successfully identified a diverse spectrum of eigenfrequencies supported by the medium. As anticipated, the calculated eigenmodes exhibit a clear evolutionary transition, while some modes remain tightly localized as WGMs around individual microspheres, others manifest as spatially extended, complex field distributions. These extended modes are indicative of strong resonant coupling between adjacent microspheres within the aggregates (Fig. 5(d and g) and (e and h)), providing the necessary theoretical foundation for the transition from localized feedback to collective random lasing.

This simulated behavior aligns perfectly with our experimental observations, confirming that large stochastic aggregates provide an expansive network of potential light amplification pathways. This structural complexity results in a significantly higher contribution of longer optical path lengths, as evidenced by the Fourier transform analysis. Consequently, the random lasing observed in these systems does not merely arise from diffuse scattering, but rather originates from individual macro-aggregates acting as complex, multimodal resonant entities, effectively a spatial and spectral superposition of multiple, strongly coupled micro-resonators.

Conclusions

This study demonstrates a robust methodology for the precise manipulation of light emission in colloidal micro-assemblies by governing the transition from order to programmable structural disorder. By leveraging the frustrated self-assembly of hollow silica microspheres within a polymer matrix, we achieved a seamless, tunable transition from localized microresonator lasing to fully developed random lasing simply by modulating the microsphere packing fraction. This transition is fundamentally driven by an evolution in the dominant optical feedback mechanism: shifting from isolated resonant feedback at low concentrations to collective multiple scattering within dense, stochastic aggregates at higher densities.

Systematic analysis of the transport mean free path (lt) and the spectral density derived from Fourier transform analysis confirms this shift, revealing the emergence of an expansive network of coupled optical resonators that sustain robust random lasing. We show that while silica microspheres can form locally ordered systems for discrete lasing, their inherent polydispersity and concentration-dependent aggregation provide a versatile platform for introducing the entropy necessary to facilitate random lasing.

Beyond serving as tunable, multi-regime light sources, the unique stochastic emission fingerprints of these aggregates are ideally suited for advanced photonic applications. Specifically, their complex spectral signatures provide a foundation for Physically Unclonable Functions (PUFs) in high-security cryptography and authentication. These results underscore that combining the principles of self-assembly with the strategic implementation of structural disorder enables the precise tailoring of complex photonic properties for next-generation optical technologies.

Conflicts of interest

There are no conflicts to declare.

Data availability

The data that support the findings of this study are available from the corresponding author upon reasonable request.

Supplementary information (SI) is available. See DOI: https://doi.org/10.1039/d6tc00581k.

Acknowledgements

This work was supported by the statutory funding of Faculty of Chemistry, Wroclaw University of Science and Technology.

References

1 K. J. Vahala, *Nature*, 2003, **424**, 839–846.
2 P. Cheben, R. Halir, J. H. Schmid, H. A. Atwater and D. R. Smith, *Nature*, 2018, **560**, 565–572.
3 E. Yablonovitch, *Phys. Rev. Lett.*, 1987, **58**, 2059.
4 S. John, *Phys. Rev. Lett.*, 1987, **58**, 2486.
5 D. S. Wiersma, *Nat. Photonics*, 2013, **7**, 188–196.
6 P. Sebbah, *Waves and imaging through complex media*, Springer Science & Business Media, 2001.

7 D. S. Wiersma, *Nat. Phys.*, 2008, **4**, 359–367.
8 H. Cao, *Waves Random Media*, 2003, **13**, R1.
9 N. M. Lawandy, R. Balachandran, A. Gomes and E. Sauvain, *Nature*, 1994, **368**, 436–438.
10 M. S. Leanenia, E. Lutsenko and G. Yablonskii, *Nano-Structures for Optics and Photonics: Optical Strategies for Enhancing Sensing, Imaging, Communication and Energy Conversion*, Springer, 2014, pp. 525–526.
11 B. Redding, M. A. Choma and H. Cao, *Nat. Photonics*, 2012, **6**, 355–359.
12 S. Knitter, C. Liu, B. Redding, M. K. Khokha, M. A. Choma and H. Cao, *Optica*, 2016, **3**, 403–406.
13 A. P. Schlaus, M. S. Spencer, K. Miyata, F. Liu, X. Wang, I. Datta, M. Lipson, A. Pan and X.-Y. Zhu, *Nat. Commun.*, 2019, **10**, 265.
14 K. Vynck, M. Burresi, F. Riboli and D. S. Wiersma, *Nat. Mater.*, 2012, **11**, 1017–1022.
15 J. D. Joannopoulos, P. R. Villeneuve and S. Fan, *Nature*, 1997, **386**, 143–149.
16 H. Cao, Y. Zhao, S. Ho, E. Seelig, Q. Wang and R. Chang, *Phys. Rev. Lett.*, 1999, **82**, 2278.
17 G. M. Conley, M. Burresi, F. Pratesi, K. Vynck and D. S. Wiersma, *Phys. Rev. Lett.*, 2014, **112**, 143901.
18 S. F. Liew, J.-K. Yang, H. Noh, C. F. Schreck, E. R. Dufresne, C. S. O'Hern and H. Cao, *Phys. Rev. A: At., Mol., Opt. Phys.*, 2011, **84**, 063818.
19 L. Sznitko, A. Szukalski, K. Cyprych, P. Karpinski, A. Miniewicz and J. Mysliwiec, *Chem. Phys. Lett.*, 2013, **576**, 31–34.
20 H. Yabu, T. Higuchi and H. Jinnai, *Soft Matter*, 2014, **10**, 2919–2931.
21 F. Serafin, J. Lu, N. Kotov, K. Sun and X. Mao, *Nat. Commun.*, 2021, **12**, 4925.
22 N. Vogel, M. Retsch, C.-A. Fustin, A. Del Campo and U. Jonas, *Chem. Rev.*, 2015, **115**, 6265–6311.
23 P. D. Garca, R. Sapienza, Á. Blanco and C. López, *Adv. Mater.*, 2007, **19**, 2597–2602.
24 K. Vynck, R. Pierrat, R. Carminati, L. S. Froufe-Pérez, F. Scheffold, R. Sapienza, S. Vignolini and J. J. Sáenz, *Rev. Mod. Phys.*, 2023, **95**, 045003.
25 Z. Wang, M. Cao, G. Shao, Z. Zhang, H. Yu, Y. Chen, Y. Zhang, Y. Li, B. Xu and Y. Wang, *et al.*, *J. Phys. Chem. Lett.*, 2020, **11**, 767–774.
26 S. A. Schulz, R. Oulton, M. Kenney, A. Alù, I. Staude, A. Bashiri, Z. Fedorova, R. Kolkowski, A. F. Koenderink and X. Xiao, *et al.*, *Appl. Phys. Lett.*, 2024, **124**, 260701.
27 M. Trivedi, D. Saxena, W. K. Ng, R. Sapienza and G. Volpe, *Nat. Phys.*, 2022, **18**, 939–944.
28 V. D. Ta, S. Caixeiro, D. Saxena and R. Sapienza, *Adv. Photonics Res.*, 2021, **2**, 2100036.
29 V. Lotito and T. Zambelli, *Adv. Colloid Interface Sci.*, 2017, **246**, 217–274.
30 Z. Cai, Z. Li, S. Ravaine, M. He, Y. Song, Y. Yin, H. Zheng, J. Teng and A. Zhang, *Chem. Soc. Rev.*, 2021, **50**, 5898–5951.
31 R. R. Syms, E. M. Yeatman, V. M. Bright and G. M. Whitesides, *J. Microelectromech. Syst.*, 2003, **12**, 387–417.
32 V. A. Marichev, *J. Solid State Electrochem.*, 2012, **16**, 3675–3681.
33 X. Xu, A. Jagota and C.-Y. Hui, *Soft Matter*, 2014, **10**, 4625–4632.
34 Z. Adamczyk, *Surface and colloid science*, Springer, 2004, pp. 211–360.
35 J. N. Israelachvili, *Intermolecular and surface forces*, Academic press, 2011.
36 P. A. Kralchevsky, K. D. Danov and N. D. Denkov, *Handbook of surface and colloid chemistry*, 1997, vol. 2.
37 D. Wang, Z. Hu, G. Peng and Y. Yin, *Nanomaterials*, 2021, **11**, 686.
38 G. Gardi and M. Sitti, *Phys. Rev. Lett.*, 2023, **131**, 058301.
39 N. L. Smith, A. Coukouma, S. Dubnik and S. A. Asher, *Phys. Chem. Chem. Phys.*, 2017, **19**, 31813–31822.
40 V. Lotito and T. Zambelli, *J. Colloid Interface Sci.*, 2015, **447**, 202–210.
41 V. Lotito and T. Zambelli, *Adv. Colloid Interface Sci.*, 2020, **284**, 102252.
42 K. Zhong, J. Li, L. Liu, S. Van Cleuvenbergen, K. Song and K. Clays, *Adv. Mater.*, 2018, **30**, 1707246.
43 D.-S. Liu, J. Wu, H. Xu and Z. Wang, *Adv. Mater.*, 2021, **33**, 2003733.
44 D. Yu, M. Humar, K. Meserve, R. C. Bailey, S. N. Chormaic and F. Vollmer, *Nat. Rev. Methods Primers*, 2021, **1**, 83.
45 K. Sobczyk and D. J. Kirkner, *Stochastic modeling of microstructures*, Springer Science & Business Media, 2001.
46 J. Andreasen, A. Asatryan, L. Botten, M. Byrne, H. Cao, L. Ge, L. Labonté, P. Sebbah, A. Stone and H. E. Türeci, *et al.*, *Adv. Opt. Photonics*, 2010, **3**, 88–127.
47 K. Zhong, K. Song and K. Clays, *Nanophotonics*, 2018, **7**, 693–713.
48 C. Zhou, X. Han and L. Bi, *Opt. Express*, 2023, **31**, 24183–24193.
49 L. Ryglowski, K. Cyprych and J. Mysliwiec, *Opt. Commun.*, 2022, **510**, 127939.
50 K. Cyprych, P. Karpinski, L. Sznitko, A. Miniewicz and J. Mysliwiec, *Opt. Mater.*, 2022, **128**, 112322.
51 A. Dorodnyy, J. Smajic and J. Leuthold, *Laser Photonics Rev.*, 2023, **17**, 2300055.
52 R. Stoian and J.-P. Colombier, *Nanophotonics*, 2020, **9**, 4665–4688.
53 H. Zhu, Z. He, J. Wang, W. Zhang, C. Pei, R. Ma, J. Zhang, J. Wei and W. Liu, *Ann. Phys.*, 2024, **536**, 2400112.
54 M. Hohmann, M. Späth, D. Ni, D. Dörner, B. Lengenfelder, F. Klämpfl and M. Schmidt, *Biomed. Opt. Express*, 2021, **12**, 5439–5451.
55 L. Fu, Q. Ma, K. Liao, J. An, J. Bai and Y. He, *Nanotechnol. Rev.*, 2022, **11**, 26–39.
56 S. Wang, W. Zhang, N. Yang, R. Ma, Y. Zhang, Z. Wang, J. Zhang and Y. Rao, *Ann. Phys.*, 2021, **533**, 2100390.

